

Quantum-Fluctuation-Frustrated Flat Band Instabilities in NdNiO₂

Mi-Young Choi¹, Warren E. Pickett^{2,*} and Kwan-Woo Lee^{1,3†}

¹*Department of Applied Physics, Graduate School, Korea University, Sejong 30019, Korea*

²*Department of Physics, University of California Davis, Davis CA 95616, USA*

³*Division of Display and Semiconductor Physics, Korea University, Sejong 30019, Korea*

(Dated: May 8, 2020)

The discovery that Nd_{1-x}Sr_xNiO₂, with the CaCuO₂ infinite-layer structure, superconducts up to 15 K around the hole-doping level $x=0.2$, raises many important questions about its fundamental electronic and magnetic processes. One unexplained feature is that, for $x=0$ and as opposed to CaCuO₂, NdNiO₂ with the same formal d^9 configuration does not order antiferromagnetically (AFM). We study the experimentally inaccessible AFM phase, finding for the static lattice, a flat-band, one-dimensional van Hove singularity (vHs) pinned to the Fermi level is unstable to charge, spin, and lattice orders. These flat-band instabilities thereby limit incipient AFM order at low temperature and, being assisted by zero point fluctuations of the oxygen lattice, preclude the AFM phase seen in CaCuO₂. This strongly AFM correlated, conducting spin-liquid phase forms the platform for superconductivity in NdNiO₂.

A disparate variety of interacting models[1–13] based on density functional theory (DFT) studies[14–21] have been proposed to illuminate the electronic and magnetic behavior underlying the discovery[22] and experimental study[23–25] of long-sought superconductivity in a layered nickelate, specifically hole-doped NdNiO₂ (NNO). With the same infinite-layer structure as CaCuO₂ (CCO), which superconducts up to 110 K when doped,[26] NNO displays several differences with CCO. Undoped NNO is conducting; CCO is insulating; CCO orders antiferromagnetically, whereas no signature of order is seen in NNO (and its iso-electronic but non-superconducting sister[27–30] LaNiO₂ [LNO]) and there is no sign of heavy fermion screening of Ni moments. CCO and NNO have a common d^9 (formal) configuration (one hole) on the transition metal ion, however NNO persists as conducting to low temperature. Central differences include positioning of metal 3d levels relative to O 2p levels that is substantially different in the two compounds, and the presence of Nd 5d character at the Fermi level.

The electronic structures of the d^9 infinite layer cuprates and nickelates were compared some time ago, with some similarities but substantial differences being noted[14–16] and quantified more recently by Wannier function analysis,[17, 18] and some impact of the Nd moments has been noted.[19] The similarities but substantial difference continue to dominate the discussion and inform the models cited above. No items however seem as fundamental as the difference in ground states of the undoped materials: antiferromagnetic (AFM) insulator for CCO, and disordered moment conductor for NNO, the latter being a conducting quantum paramagnetic (MQPM) phase in the Sachdev-Read classification.[31] Based on an interacting two-band model, Werner and

Hoshino[4] discussed NNO in terms of the spin-freezing theory of unconventional superconductivity,[32, 33] and the potentially simpler case of superconductivity at high pressure in elemental Eu with disordered f^7 moments[34] might share in this behavior.

Here we focus on this absence of (AFM) ordering of Ni moments in NNO, moments whose ordering has been the overriding hallmark of the undoped phase in cuprates. In closely related layered nickelates[35–39] (*viz.* La₃Ni₂O₆, La₄Ni₃O₈, La₄Ni₃O₁₀) even with non-integral formal Ni valences magnetic ordering and sometimes charge ordering occur; none has a ground state without symmetry breaking, unlike NNO. In spite of being energetically favored in the absence of fluctuations (*i.e.* in DFT calculations[15, 18, 19]), the ordered state (with $S=1$ quantum fluctuations) is not observed, hence it is a metastable but physically inaccessible phase. The AFM state of NNO is however accessible computationally, allowing study of its electronic structure and microscopic processes that oppose further symmetry breaking, thereby giving insight into the inaccessibility of the AFM phase.

We adopt the DFT plus anisotropic Coulomb U (DFT+ U) method[40] as implemented in WIEN2K[41] as described in our previous work,[19] retaining the all-electron character of Nd which provides Nd $d-f$ exchange coupling but is not the subject here. Details of the frozen phonon studies are provided in the Supplemental Material (SM)[42]. We use Hund's exchange coupling $J_{Ni}^H = 0.7$ eV throughout, and quote values of U_{Ni}^d (simply called U) that we explore.

Energies and moments. The AFM state we study has both antialigned Nd and Ni spin layers, with no net near neighbor Nd-Ni coupling. This AFM ordering is energetically favored over aligned Ni spins by 95 (62) meV/f.u. at $U = 0(4)$ eV, both being strongly favored over non-magnetic Ni.[18, 19] No theoretical value of the energy for disordered moments is available, but would be of the order of J_{Ni}^H . Although DFT often overestimates magnetic moments and thereby energies in weak magnets, it is

*Electronic address: wepickett@ucdavis.edu

†Electronic address: mckwan@korea.ac.kr

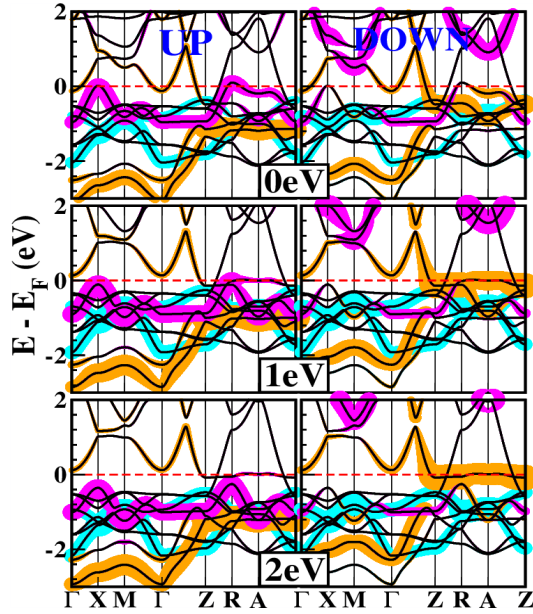


FIG. 1: Fatband depiction of the AFM band structure in GGA+U: (Left) Ni majority; (right) Ni minority. Panels are for $U=0, 1, 2$ eV as noted, with $E_F \equiv 0$. The flat d_{z^2} band appears along the $Z-R-A-Z$ lines ($k_z = \pi/c$ zone face) already for $U=1$ eV. Ni d_{z^2} , $d_{x^2-y^2}$, and d_{xy} characters (described in the primitive cell) are highlighted by brown, pink, and green colors, respectively. Relative to the primitive cell, symmetry points are rotated by 45° in the $\sqrt{2} \times \sqrt{2}$ AFM supercell, *i.e.*, $M(R) \leftrightarrow X(A)$.

commonly accurate for larger (ionic) moments. These Ni moments are $\sim 1\mu_B$ or more, characteristic of hybridized $S=1/2$ moments but only if hybridization with oxygen is strong or a second orbital is involved. Adding the effect of U revises the energetics and increases the moments, but not the relative stabilities of AMF and FM order. The observed avoidance by NNO of a relatively large ordering energy is our focus.

Correlation effects and the flat band. Correlation effects are immediate and unexpected. Including even a small value of U leads to a dramatic change in the Ni d_{z^2} -derived band below but very near the Fermi energy E_F . Figure 1 shows in fatband form the Ni d_{z^2} , $d_{x^2-y^2}$, and d_{xy} band characters as U increases over the range 0–2 eV; d_{xz} , d_{yz} orbitals of both spin are occupied. At $U=0$, all three orbitals are active near E_F . However, already with the modest value $U=1$ eV, an unanticipated flat band emerges to E_F along the entire zone face $k_z = \pi/c$ ($Z-A-R-Z$ lines). This distinctive electronic feature remains in place as U increases to 5 eV. To emphasize: the flat band on the upper/lower zone face is a robust feature of AFM order, with implications discussed below.

The relatively short Ni-Ni distance along the c -axis induces a hopping (assisted by Nd d_{z^2} and d_{xy}) between the d_{z^2} orbitals on nearby layers, leading to dispersion of 2 eV along the $\Gamma-Z$ line. The related effective hopping

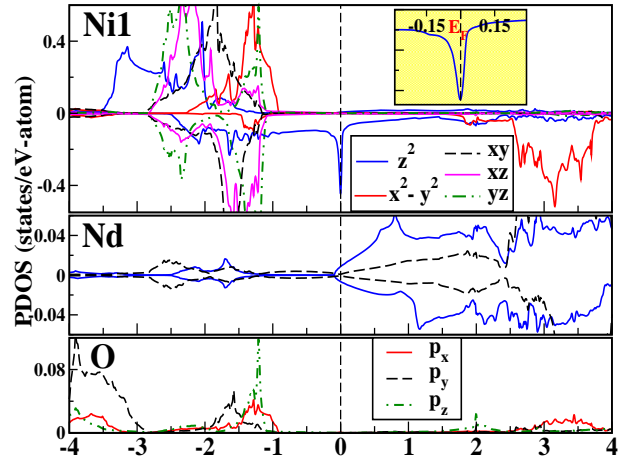


FIG. 2: AFM orbital-projected densities of states (PDOSs)/atom of Ni 3d, two Nd 5d d_{z^2} and d_{xy} orbitals, and O 2p orbitals, for the undistorted lattice at $U = 4$ eV, in the 3d band region (note the difference in scales). Majority (minority) are plotted upward (downward). The oxygen PDOS lies below 3 eV. Having E_F pinned precisely at the sharp, 1D-like vHs (upper panel, minority spin, shown enlarged in the Inset) produces the instabilities discussed in the text.

parameter is $t_{z^2} \approx 1$ eV, large for k_z hopping across a 10\AA distance. For the minority (higher energy) states, the Ni d_{z^2} orbital is mixed with Nd d_{xy} and somewhat with Nd $d_{x^2-y^2}$ on the $k_z = \pi/c$ plane, resulting in a hybridization gap of 0.4 eV at the Z -point. The mixtures elsewhere, *viz.* at Γ , are negligible.

Figure 2 shows (for the realistic metallic value $U=4$ eV) Ni, Nd, and O orbital-projected densities of states (PDOSs) in the d band region surrounding E_F . The unfilled minority Ni $d_{x^2-y^2}$ orbital (the hole) lies at +3 eV. One remarkable feature is that the minority Ni d_{z^2} band spans nearly 5 eV, crossing E_F and ensuring a conducting state. All other Ni d orbitals of both spins are narrow. The other notable feature is that this same orbital gives rise to a flat band across the entire $k_z = \pi/c$ zone face that produces a 1D van Hove singularity (vHs) *pinned at E_F* , with pure d_{z^2} character; recall, these two exotic features are robust, that is, insensitive to U . The valence bands have nearly pure Ni d_{z^2} character within 1 eV of E_F . Nd 5d character extends down to and slightly below E_F as noted several times previously, but does not participate in the flat band. Around Z (see along the $Z-R$ and $Z-A$ lines in Fig. 1), the flat band crosses a dispersive band with mixed Nd $5d_{z^2}$, Nd $3d_{xz/yz}$ character at E_F .

As a result of coupling through Nd states, the flat band acquires a small width ~ 40 meV corresponding to an effective *in-plane* hopping $t_{z^2}^{eff} = 20$ meV for this plane. Based on charge decompositions and PDOSs, and the Ni d_{z^2} character above E_F , the evidence suggests a formal valence closer to $\text{Ni}^{1.4+}$ rather than Ni^{1+} as would be appropriate for an insulator. (Since O is clearly $2-$, we expect this is a breakdown of formal valence counting as

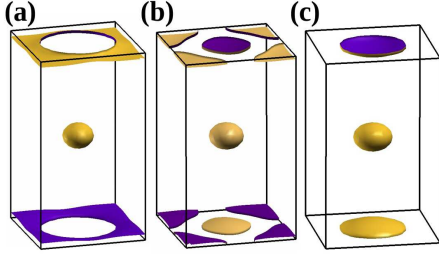


FIG. 3: Variations of Fermi surfaces by carrier dopings: (a) 0.025 hole-doping, (b) undoped, and (c) 0.025 electron-doping per f.u. at $U = 4.0$ eV. The doping cases were treated with the virtual crystal approximation by replacing the atomic number of Nd.

often occurs in metals.) In contrast to cuprates where the central role implicates the Cu $d_{x^2-y^2}$ orbital, our results support previous indications[15] that the Ni d_{z^2} orbital becomes a central player in NNO (and LNO), with the $d_{x^2-y^2}$ hole being more of a given and less of a dynamical component.

Fermi surfaces versus doping. The Fermi surfaces (FSs) for $U = 4$ eV versus small (virtual crystal) doping levels are shown in Fig. 3. A Γ -centered electronic sphere, a mixture of Ni $3d_{z^2}$ and Nd $5d_{z^2}$ character,[15, 19] arises from the high velocity band. Quasi-1D pieces emerge on the $k_z = \pi/c$ plane. For hole-doping, the thin hole wafer is pinched off around the Z-point (Fig. 3(a)). At stoichiometry, Fig. 3(b), the hole FS shrinks and flat electron buttons appear around the Z point, leaving rounded-diamond hole buttons at the zone vertices. Small electron doping, Fig. 3(c), leads to electron buttons around Z; the electron sphere at Γ is simply changed in volume during low doping.

The thin button FSs have a characteristic thickness $\Delta k_z \leq 0.06\frac{\pi}{c}$ or less, providing nesting that would encourage charge- or spin-density waves (or related Kohn anomalies) of wavelength greater than $2\pi/\Delta k_z \sim 8c$, supported by nesting extending over a range of parallel q components. Such long wavelength fluctuations are difficult numerically to explore.

Magnetic Instability. To probe the Stoner instability in this already magnetically-ordered AFM state, we use lattice displacements [Fig. 4(a)] to break symmetry. The changes in moments of the Ni1 and Ni2 sites are displayed in Fig. 4(b). Unexpectedly, tiny mode amplitudes (displacements down to 0.001\AA extrapolating to zero) produce a ‘spin disproportionation’ of the order of $\pm 0.05 \mu_B$. To clarify: the AFM state is unstable to a first order transition to a *ferrimagnetic* state, which reflects the partially itinerant character of the Ni moments. The mechanism is the vHs/Stoner instability, with feedback within the self-consistency loop (necessitated by the vHs) providing the first order stabilization; actual lattice distortion is unnecessary. The magnetic symmetry breaking is accompanied by a Ni1-to-Ni2 charge transfer up to $\sim \pm 0.05e$ (from atomic sphere charges).

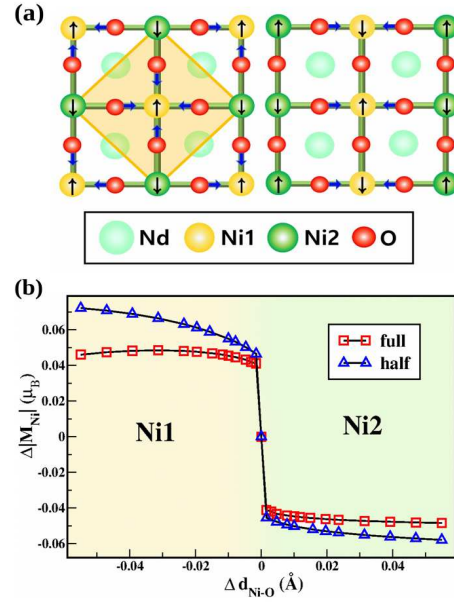


FIG. 4: (a) Sketch of the NiO_2 layer with (left) oxygen full-breathing mode and (right) half-breathing mode along (100) direction, showing 2×2 primitive cells. The full- and half-breathing modes allow for checkerboard and stripe charge and spin orders, respectively. The arrows on the Ni ions indicate spins of Ni ions, whereas the blue (thick) arrows denote the displacement of oxygen ions. (b) Changes of the magnitude of Ni magnetic moments ΔM , versus changes in the Ni-O bond length $\Delta d_{\text{Ni-O}}$ for both the full- and half-breathing modes at $U = 4$ eV. This ‘spin disproportionation’ instability occurs for the undistorted lattice. There is an accompanying charge disproportionation (see text).

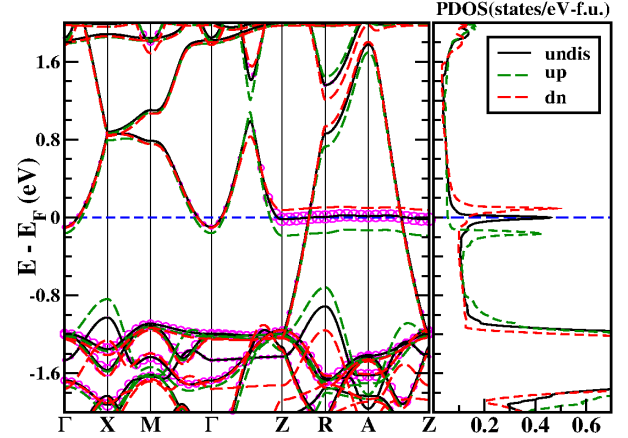


FIG. 5: AFM band structures and Ni atom-PDOSs for $U = 4$ eV. The (red and green) dashed lines indicate the bands split by the full-breathing mode, with O displaced by 0.03\AA . The half-breathing mode (not shown) shows similar band splitting. The peak-splitting is the source of the Peierls (Stoner) charge (spin) instability.

Lattice Instability. The effect of the breathing mode on the band structure is displayed in Fig. 5, quantify-

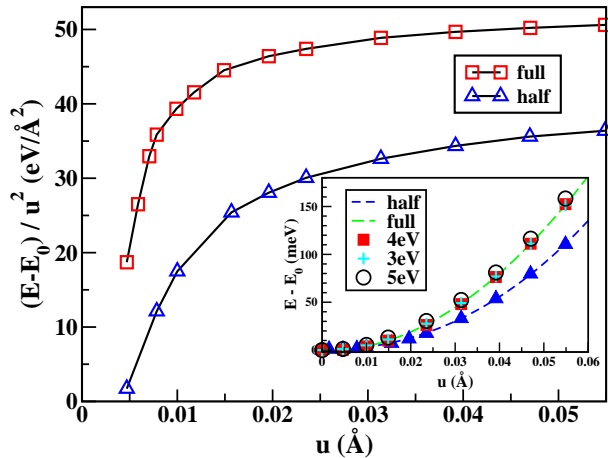


FIG. 6: Energy distortions for the frozen-in oxygen full- and half-breathing modes at $U = 4$ eV. As shown in the Inset, these follow a quadratic plus lowest-order anharmonic term, indicated by the green (blue) dashed lines, and are insensitive to strength of U in the range of 3 - 5 eV.

ing the splitting of the vHs peak. This splitting defines a deformation potential: peak splitting per unit distortion,[43] see the SM for more information[42]. To explore the Peierls lattice instability, we plot the energy difference divided by squared amplitude ($\Delta E(u)/u^2$) in Fig. 6; this is the lattice stiffness. If calculated as usual on a mesh of u of 0.01, 0.02, 0.03 Å etc., one would conclude stable, in fact, high energy modes of $\omega = 79$ meV and 62 meV for the full- and half-breathing modes, respectively (Fig. 4(a)), with evidence of some anharmonicity. Compared with the values in CaCuO_2 [44] and in La_2CuO_4 [45], these frequencies are reduced by 11%-23% respectively.

The sharp and narrow vHs however negates normal charge response and provides a platform that is extremely sensitive to any symmetry breaking that splits the vHs peak. The anomalous response is confined to small distortions and energies (and temperature). Figure 6 shows that as the amplitude u is decreased below 0.015 Å, the lattice stiffness dives to lower values and extrapolates to negative values below $u = 0.004$ Å. This is the classic Peierls instability, and a full treatment (unnecessary here) would require self-consistent theory of non-adiabatic electron-lattice coupling, where heavy charge

carriers are coupled to phonons of similar energy.

However, there is oxygen zero point motion to account for. For frequencies of 60-80 meV, the oxygen zero point amplitude $\langle u_0 \rangle \approx 0.06$ Å is four times larger than the region of non-adiabatic behavior (Fig. 6), so this quantum fluctuation will frustrate the static lattice instability, and quench the spin and charge orders as well. How the massive carriers would deal with all of these frustrated instabilities promises to be a challenging theoretical problem, but the outcome is that the underlying AFM order we have modeled gives way to a disordered moment metal.

Discussion: avoidance of the AFM phase. We have studied the experimentally inaccessible AFM ordered state of NdNiO_2 with correlated DFT methods. This is the state whose calculated energy indicates it should be the ground state versus the observed disordered moment state. We found that a Ni d_{z^2} flat band arises on the entire $k_z = \pi/c$ zone face, giving a 1D-like vHs that supports (neglecting fluctuations) spin, charge, and lattice (breathing and half-breathing mode) instabilities of the ideal infinite-layer lattice. Due to the narrowness of the vHs, these coupled order parameters are sensitive to quantum zero point oxygen motion and non-adiabatic electron-lattice coupling in the vHs peak, finally frustrating these types of lowering of symmetry.

Yet the AFM ordered state, calculated to be most stable for the static lattice, remains inaccessible by experiment, *i.e.* higher in free energy than the spin-disordered, spin liquid state. We propose that as temperature is lowered NdNiO_2 approaches the AFM ordered phase but encounters its incipient instabilities with strong spin and charge fluctuations that inhibits spin order. The result is to remain spin-disordered but with strong long range correlations, *i.e.* incipient AFM order, that reduce the free energy. This correlated spin liquid phase, the Sachdev-Read MQPM phase that has been proposed in another disordered moment superconductor,[34] provides the platform for the superconductivity that appears upon hole doping.

Acknowledgments

M.Y.C. and K.W.L. were supported by National Research Foundation of Korea Grant No. NRF-2019R1A2C1009588. W.E.P. was supported by NSF Grant No. DMR 1607139.

-
- [1] L.-H. Hu and C Wu, Two-band model for magnetism and superconductivity in nickelates, *Phys. Rev. Research* **1**, 032046 (2019).
 - [2] S. Ryee, H. Yoon, T. J. Kim, M. Y. Jeong, and M. J. Han, Induced magnetic two-dimensionality by hole doping in the superconducting infinite-layer nickelate $\text{Nd}_{1-x}\text{Sr}_x\text{NiO}_2$, *Phys. Rev. B* **101**, 064513 (2020).
 - [3] X. Wu, D. D. Sante, T. Schwemmer, W. Hanke, H. Y. Hwang, S. Raghu, and R. Thomale, Robust $d_{x^2-y^2}$ -wave

superconductivity of infinite-layer nickelates, *Phys. Rev. B* **101**, 060504(R) (2020).

- [4] P. Werner and S. Hoshino, Nickelate superconductors: Multiorbital nature and spin freezing, *Phy. Rev. B* **101**, 041104(R) (2020).
- [5] G.-M. Zhang, Y.-F. Yang, and F.-C. Zhang, Self-doped Mott insulator for parent compounds of nickelate superconductors, *Phys. Rev. B* **101**, 020501(R) (2020).
- [6] F. Lechermann, Late transition metal oxides with infinite-

- layer structure: Nickelates versus cuprates, *Phys. Rev. B* **101**, 081110(R) (2020).
- [7] H. Zhang, L. Jin, S. Wang, B. Xi, X. Shi, F. Ye, and J.-W. Mei, Effective Hamiltonian for nickelate oxides $\text{Nd}_{1-x}\text{Sr}_x\text{NiO}_2$, *Phys. Rev. Research* **2**, 013214 (2020).
 - [8] H. Sakakibara, H. Usui, K. Suzuki, T. Kotani, H. Aoki, and K. Kuroki, Model construction and a possibility of cuprate-like pairing in a new d^9 nickelate superconductor $(\text{Nd,Sr})\text{NiO}_2$, arXiv:1909.00060.
 - [9] Y. Gu, S. Zhu, X. Wang, J. Hu, and H. Chen, Hybridization and correlation effects in the electronic structure of infinite-layer nickelates, arXiv:1911.00814.
 - [10] J. Chang, J. Zhao, and Y. Ding, Hund-Heisenberg model in superconducting infinite-layer nickelates, arXiv:1911.12731.
 - [11] M. Jiang, M. Berciu, and G. A. Sawatzky, The critical nature of the Ni spin state in doped NdNiO_2 , arXiv:1909.02557.
 - [12] T. Zhou, Y. Gao, and Z. D. Wang, Spin excitations in nickelate superconductors, arXiv:1910.05757.
 - [13] J. Karp, A. S. Botana, M. R. Norman, H. Park, M. Zingl, and A. Millis, Many-body Electronic Structure of NdNiO_2 and CaCuO_2 , arXiv: 2001.06441.
 - [14] V. I. Anisimov, D. Bukhvalov, and T. M. Rice, Electronic structure of possible nickelate analogs to the cuprates, *Phys. Rev. B* **59**, 7901 (1999).
 - [15] K.-W. Lee and W. E. Pickett, Infinite-layer nickelates LaNiO_2 : Ni^{1+} is not Cu^{2+} , *Phys. Rev. B* **70**, 165109 (2004).
 - [16] P. Jiang, L. Si, Z. Liao, and Z. Zhong, Electronic structure of rare-earth infinite-layer RNiO_2 ($\text{R}=\text{La}, \text{Nd}$), *Phys. Rev. B* **100**, 201106(R) (2019).
 - [17] Y. Nomura, M. Hirayama, T. Tadano, Y. Yoshimoto, K. Nakamura, and R. Arita, Formation of a two-dimensional single-component correlated electron system and band engineering in the nickelate superconductor NdNiO_2 , *Phys. Rev. B* **100**, 205138 (2019).
 - [18] A.S. Botana and M.R. Norman, Similarities and Differences between LaNiO_2 and CaCuO_2 and Implications for Superconductivity, *Phys. Rev. X* **10**, 011024 (2020).
 - [19] M.-Y. Choi, K.-W. Lee, and W. E. Pickett, Role of 4f states in infinite-layer NdNiO_2 , *Phys. Rev. B* **101**, 020503(R) (2020).
 - [20] Z. Liu, Z. Ren, W. Zhu, Z. F. Wang, and J. Yang, Electronic and Magnetic Structure of Infinite-layer NdNiO_2 : Trace of Antiferromagnetic Metal, arXiv:1912.01332.
 - [21] B. Geisler and R. Pentcheva, Fundamental difference in the electronic reconstruction of infinite-layer vs. perovskite neodymium nickelate films on $\text{SrTiO}_3(001)$, arXiv:2001.03762.
 - [22] D. Li, K. Lee, B. Y. Wang, M. Osada, S. Crossley, H. R. Lee, Y. Cui, Y. Hikita, and H. Y. Hwang, Superconductivity in an infinite-layer nickelate, *Nature* **572**, 624 (2019).
 - [23] M. Hepting *et al.*, Electronic structure of the parent compound of superconducting infinite-layer nickelates, *Nat. Mater.* **19**, 381 (2020).
 - [24] Q. Li, C. He, J. Si, X. Zhu, Y. Zhang, and H.-H. Wen, Absence of superconductivity in bulk $\text{Nd}_{1-x}\text{Sr}_x\text{NiO}_2$. *Commun. Mater.* **1**, 16 (2020).
 - [25] Y. Fu *et al.*, Core-level x-ray photoemission and Raman spectroscopy studies on electronic structures in Mott-Hubbard type nickelate oxide NdNiO_2 , arXiv:1911.03177.
 - [26] M. Azuma, Z. Hiroi, M. Takano, Y. Bando, and Y. Tekeda, Superconductivity at 110K in the infinite-layer compound $(\text{Sr}_{1-x}\text{Ca}_x)_{1-y}\text{CuO}_2$, *Nature* **356**, 775 (1992).
 - [27] M. Crespin, P. Levitz, and L. Gatineau, Reduced forms of LaNiO_3 perovskite. Part 1. Evidence for new phases: $\text{La}_2\text{Ni}_2\text{O}_5$ and LaNiO_2 , *J. Chem. Soc., Faraday Trans. 2* **79**, 1181 (1983).
 - [28] M. A. Hayward, M. A. Green, M. J. Rosseinsky, and J. Sloan, Sodium Hydride as a Powerful Reducing Agent for Topotactic Oxide De-intercalation: Synthesis and Characterization of the Nickel(I) Oxide LaNiO_2 , *J. Am. Chem. Soc.* **121**, 8843 (1999).
 - [29] D. Kaneko, K. Yamagishi, A. Tsukada, T. Manabe, and M. Naito, Synthesis of infinite-layer LaNiO_2 films by metal organic decomposition, *Physica C: Superconductivity* **469**, 936 (2009).
 - [30] A. Ikeda, T. Manabe, and M. Naito, Improved conductivity of infinite-layer LaNiO_2 thin films by metal organic decomposition, *Physica C: Superconductivity* **495**, 134 (2013).
 - [31] S. Sachdev and N. Read, Metallic spin glasses, *J. Phys.: Condens. Matt.* **8**, 9723 (1996).
 - [32] S. Hoshino and P. Werner, Superconductivity from Emerging Magnetic Moments, *Phys. Rev. Lett.* **115**, 247001 (2015).
 - [33] P. Werner, S. Hoshino, and H. Shinaoka, Spin-freezing perspective on cuprates, *Phys. Rev. B* **94**, 245134 (2016).
 - [34] S.-T. Pi, S. Y. Savrasov, and W. E. Pickett, Pressure-tuned frustration of Magnetic Coupling in Elemental Europium, *Phys. Rev. Lett.* **122**, 057201 (2019).
 - [35] V. Pardo and W. E. Pickett, Metal-insulator transition in layered nickelates $\text{La}_3\text{Ni}_2\text{O}_{8-\delta}$ ($\delta = 0.0, 0.5, 1$), V. Pardo and W. E. Pickett, *Phys. Rev. B* **83**, 245128 (2011).
 - [36] A. S. Botana, V. Pardo, W. E. Pickett, M. R. Norman, Charge ordering in $\text{Ni}^{1+}/\text{Ni}^{2+}$ nickelates: $\text{La}_4\text{Ni}_3\text{O}_8$ and $\text{La}_3\text{Ni}_2\text{O}_6$, *Phys. Rev. B* **94**, 081105(R) (2016).
 - [37] J. Zhang, A. S. Botana, J. W. Freeland, D. Phelan, H. Zheng, V. Pardo, M. R. Norman, J. F. Mitchell, Mimicking cuprates: large orbital polarization in a metallic square-planar nickelate, *Nature Physics* **13**, 864 (2017).
 - [38] A. S. Botana, V. Pardo, and M. R. Norman, Electron doped layered nickelates: spanning the phase diagram of the cuprates, *Phys. Rev. Materials* **1**, 021801 (2017).
 - [39] J. Zhang *et al.*, Spin stripe order in a square planar trilayer nickelate, *Phys. Rev. Lett.* **122**, 247201 (2019).
 - [40] E. R. Ylvisaker, K. Koepf, and W. E. Pickett, Anisotropy and magnetism in the LSDA+U method, *Phys. Rev. B* **79**, 035103 (2009).
 - [41] K. Schwarz and P. Blaha, Solid state calculations using WIEN2k, *Comput. Mater. Sci.* **28**, 259 (2003).
 - [42] See Supplemental Material at [URL provided by the publisher] where information is provided on the calculation methods and several results beyond those in the manuscript.
 - [43] K.-W. Lee and W. E. Pickett, Superconductivity in Boron-Doped Diamond, *Phys. Rev. Lett.* **93**, 237003 (2004).
 - [44] P. Zhang, S. G. Louie, and M. L. Cohen, Electron-Phonon Renormalization in Cuprate Superconductors, *Phys. Rev. Lett.* **98**, 067005 (2007).
 - [45] T. Fukuda, J. Mizuki, K. Ikeuchi, K. Yamada, A. Q. R. Baron, and S. Tsutsui, Doping dependence of softening in the bond-stretching phonon mode of $\text{La}_{2-x}\text{Sr}_x\text{CuO}_4$ ($0 \leq x \leq 0.29$), *Phys. Rev. B* **71**, 060501(R) (2005).